Published in final edited form as:
J Med Chem. 2010 April 22; 53(8): 3389–3395. doi:10.1021/jm1000979.

N-((1-Benzyl-1*H*-1,2,3-triazol-4-yl)methyl)arylamide as a New Scaffold that Provides Rapid Access to Antimicrotubule Agents: Synthesis and Evaluation of Antiproliferative Activity Against Select Cancer Cell Lines

Jonathan A. Stefely[†], **Rahul Palchaudhuri**[‡], **Patricia A. Miller**[†], **Rebecca J. Peterson**[†], **Garrett C. Moraski**[†], **Paul J. Hergenrother**[‡], and **Marvin J. Miller**[*,†]

[†]Department of Chemistry and Biochemistry, University of Notre Dame, Notre Dame, Indiana 46556

[‡]Department of Chemistry, Roger Adams Laboratory, University of Illinois, Urbana, Illinois 61801

Abstract

A series of *N*-((1-benzyl-1*H*-1,2,3-triazol-4-yl)methyl)arylamides was synthesized by copper-catalyzed azide–alkyne cycloaddition (CuAAC) and afforded inhibitors of cancer cell growth. For example, compound **13e** had an IC_{50} of 46 nM against MCF-7 human breast tumor cells. Structure–activity relationship (SAR) studies demonstrated that (i) *meta*-phenoxy substitution of the *N*-1-benzyl group is important for antiproliferative activity and (ii) a variety of heterocyclic substitutions for the aryl group of the arylamide are tolerated. *In silico* COMPARE analysis of antiproliferative activity against the NCI-60 human tumor cell line panel revealed a correlation to clinically useful antimicrotubule agents such as paclitaxel and vincristine. This *in silico* correlation was supported by (i) in vitro inhibition of tubulin polymerization, (ii) G_2/M-phase arrest in HeLa cells as assessed by flow cytometry, and (iii) perturbation of normal microtubule activity in HeLa cells as observed by confocal microscopy. The results demonstrate that *N*-((1-benzyl-1*H*-1,2,3-triazol-4-yl)methyl)arylamide is a readily accessible small molecule scaffold for compounds that inhibit tubulin polymerization and tumor cell growth.

Keywords

Triazole; Click Chemistry; CuAAC; Antimicrotubule; Antitumor; Antiproliferative; Anticancer; Tubulin; Microtubule

Introduction

Microtubules, dynamic protein polymers composed of α-tubulin and β-tubulin heterodimers, are a well-established cellular target for anticancer drugs.[1] Dynamic polymerization of tubulin is a necessary and tightly controlled process during mitosis.[2] Perturbing microtubule dynamics with small molecules blocks the cell cycle in the metaphase/anaphase transition and leads to apoptosis.[3] Thus, molecules[4] that target tubulin halt rapid cell division, a characteristic of cancer cells.[5] This therapeutic strategy has been validated by the clinical

*To whom correspondence should be addressed. Phone: +1 574-631-7571. Fax: +1 574-631-6652. mmiller1@nd.edu.

Supporting Information Available. Materials and methods, characterization data for all compounds, cell proliferation curves, cell cycle arrest profiles, and COMPARE analysis results.

success of antimicrotubule drugs such as paclitaxel, docetaxel, vincristine, and vinblastine. Nonetheless, neurotoxicity and P-glycoprotein-mediated drug resistance limit the clinical utility of these drugs.[6] New-generation taxoids, vinca alkaloids, and other novel chemotypes that modulate microtubule dynamics have been synthesized in efforts to overcome these limitations.[7] For example, small molecule modulators of tubulin polymerization that do not elicit neurotoxicity in mice have been identified,[8] suggesting that neurotoxicity is not intrinsically linked to antimicrotubule agents. Nonetheless, few of these new antimicrotubule agents have produced useful clinical results. The key limitation to the development of new antimicrotubule drugs is a narrow therapeutic window.[9] A new antimicrotubule scaffold amenable to rapid derivatization and combinatorial library synthesis would provide an exceptional opportunity for the discovery of an efficacious antimicrotubule agent with an improved therapeutic window.

Herein we report the synthesis, in vitro antiproliferative activity against select cancer cell lines, and structure–activity relationships of compounds containing the *N*-((1-benzyl-1*H*-1,2,3-triazol-4-yl)methyl)arylamide scaffold. We also report mode of action studies based on *in silico*, in vitro and cell culture experiments, which reveal the potent antimicrotubule activity of this scaffold. The discovery of this scaffold stemmed from our work on Mycobactin S (**1**),[10] a natural product produced by *Mycobacterium smegmatis* that exhibits anti-tuberculosis activity[11] (Chart 1). All synthetic intermediates encountered during our group's total synthesis of Mycobactin S[12] were screened for biological activity. Surprisingly, benzyl ester **2**, a small fragment of the natural product, exhibited anti-tuberculosis activity similar to that of Mycobactin S. Furthermore, in contrast to Mycobactin S, compound **2** provided a scaffold that was amenable to rapid structure–activity relationship studies, which led to the discovery of more potent anti-tuberculosis agents.[13] While exploring derivatives of **2**, we found that 2-phenyl-oxazole-4-carboxamide derivative **3** was also active against *M. tuberculosis*. 2-Phenyl-oxazole-4-carboxamides are known inhibitors of histone deacetylase,[14] Stat3,[15] phosphodiesterase,[16] phosphatase,[17] thromboxane synthase,[18] and kinase proteins,[19] and known activators of cellular caspase activity.[20] We synthesized derivatives of **3** to identify a more potent anti-tuberculosis agent.[13] One of the derivatives, compound **4e**, had weak anti-tuberculosis activity, but broader biological screening serendipitously revealed that **4e** and related derivatives have potent antimicrotubule activity in cancer cells, as disclosed in this report.

Results and Discussion

Chemistry

2-Phenyl-oxazole-4-carboxylic acid **7** was synthesized according to the protocols shown in Scheme 1.[11,12] Coupling benzoyl chloride to serine benzyl ester hydrochloride afforded β-hydroxy amide **5**. Dehydrative cyclization and oxidation of β-hydroxy amide **5** with diethylaminosulfurtrifluoride (DAST) and DBU/$BrCCl_3$ yielded oxazole **6**.[22] Catalytic hydrogenolysis of the benzyl ester provided 2-phenyl-oxazole-4-carboxylic acid **7**.

Our strategy for exploring the chemical space around the 2-phenyl-oxazole-4-carboxamide fragment employed "click chemistry."[23] More specifically, we selected the Cu(I)-catalyzed azide–alkyne cycloaddition (CuAAC) reaction[24] because of its wide scope, high efficiency, and recognized utility for drug discovery.25 Following this strategy, *N*-((1-benzyl-1*H*-1,2,3-triazol-4-yl)methyl)-2-phenyl-oxazole-4-carboxamides **4a**–**e** were synthesized as shown in Scheme 2. Coupling propargylamine to freshly prepared 2-phenyloxazole-4-carboxyl chloride (derived from the corresponding carboxylic acid **7**) provided alkyne **8**. With the terminal alkyne precursor in hand, we turned our attention to the syntheses of azides **10a**–**e**. Benzyl bromides **9a**–**e** were treated with NaN_3 to afford benzyl azides **10a**–**e**.[26] Exposing terminal alkyne **8** to benzyl azides **10a**–**e** in the presence of catalytic Cu(I) produced 1,4-

disubstituted triazoles **4a**–**e** in high regioselectivity. Aqueous CuAAC conditions (H_2O/*t*-BuOH, 2:1) facilitated precipitation of the products, which were isolated with high purity.[24]

In order to explore the structure–activity relationships of the aryl amide group, a more general *N*-((1-benzyl-1*H*-1,2,3-triazol-4-yl)methyl)arylamide scaffold was synthesized according to the protocols shown in Scheme 3. The simplicity of reaction Scheme 2 and Scheme 3 is anticipated to allow the synthesis of a large library of 1,2,3-triazole-based structures. Moreover, the CuAAC reaction is the convergent synthetic step. Both the arylamide and benzyl groups, attached to opposite sides of the central triazole, are important components of the pharmacophore, as shown by the structure–activity studies described below. The convergence of the synthesis will allow both sides of the scaffold to be systematically varied in future SAR studies.

In Vitro Antiproliferative Activity

The antiproliferative activity of compounds **4a**–**e** against cancer cells was discovered during broad biological screening of a series of compounds originally anticipated to have anti-tuberculosis activity. Although compounds **4a**–**e** had negligible anti-tuberculosis activity, they inhibited the proliferation of cancer cells in vitro. Therefore, we determined the antiproliferative activities (IC_{50} values) of hit compounds **4a**–**e** against the breast tumor-derived cell line MCF-7 (Table 1). Because the IC_{50} of **4e** (0.56 μM) was significantly lower than those of **4a**–**d** (IC_{50} = 7.3–16 μM), we conserved *meta*-phenoxy benzyl substitution at triazole N-1 in the second series of analogs (Scheme 3).

The structure–activity relationships of the triazole C-4 substituent were investigated by changing the carboxamide group (Table 2). In this SAR study, antiproliferative activity was investigated with the MCF-7 cell line and human lymphoma cell line U937. Addition of electron withdrawing or electron donating groups to the *para*-position of the 2-phenyloxazole group (**13a**–**c**) had a significant effect on antiproliferative activity, revealing an avenue for future optimization. Before performing an extensive SAR study via substitution of the 2-phenyloxazole group, we wanted to know if the 2-phenyloxazole was necessary for antiproliferative activity. If simpler aryl groups could replace the 2-phenyloxazole, the three-step synthesis of the 2-phenyloxazole-4-carboxylic acids could be bypassed by using commercial aryl acids. Thus, we conducted a systematic truncation of the 2-phenyloxazole-4-carboxamide group found in **4e**. Removing the 2-phenyl group (**13d**) did not significantly change the activity. Following this lead, which suggested that we could use simpler aryl groups, we synthesized 2-pyridyl derivative **13e**. Against the MCF-7 cell line, the IC_{50} of **13e** (46 nM) was significantly lower than that of **4e** (560 nM). Likewise, a significant decrease in IC_{50} was observed with the U937 cell line. Therefore, replacing the 2-phenyloxazole group with simpler aryl groups represents a significant opportunity to improve antiproliferative activity. Phenyl derivative **13f** had improved antiproliferative activity compared to **4e**, but was less active than 2-pyridyl derivative **13e**. Replacing the aryl group with a methyl group (**14**) gave a meaningful loss of antiproliferative activity and demonstrated the importance of the aryl carboxamide group.

Time Dependence of In Vitro Cellular Antiproliferative Activity

In order to distinguish cytotoxic activity from cytostatic activity, the time dependence of the effect of **13e** on MCF-7 cells was determined (Figure 1). At a concentration of 39 nM, **13e** slowed the cell proliferation rate. At higher concentrations (78 nM and 156 nM), cellular proliferation was halted, but **13e** did not decrease the number of cells. Thus, at concentrations moderately higher than the IC_{50}, **13e** is cytostatic rather than cytotoxic against MCF-7 cells.

Broad-Spectrum In Vitro Antiproliferative Activity

The NCI-60 anticancer drug screen is an in vitro assay consisting of 60 different human tumor cell lines.[27] Organized by disease type, the NCI-60 panel includes various leukemia cell lines and cell lines derived from solid tumor sources. Cell line selectivity guides further biological evaluation. In the NCI-60 panel, compounds **4b**, **4c**, **4d**, and **4e** induced broad-spectrum antiproliferative activity against tumor cell lines derived from leukemia, non-small cell lung cancer, colon cancer, CNS cancer, melanoma, ovarian cancer, renal cancer, prostate cancer, and breast cancer (see Supplemental Information). Of these four compounds, **4e** (NCI-60 mean GI_{50} = 870 nM) was more than twenty times more potent than the other three compounds (Table 3). This result is consistent with the results from our MCF-7 and U937 assays and further emphasizes the importance of *meta*-phenoxy benzyl substitution of triazole N-1 for optimal activity within this scaffold. With respect to selectivity among the 60 cell lines in the NCI-60 panel, all four compounds tested in the panel showed greater than average potency against human leukemia cell line HL-60, breast cancer cell line MCF-7, and melanoma[28] cell line MDA-MB-435 (Table 3).

COMPARE Analysis Revealed a Correlation to Antimicrotubule Drugs

For a given compound, the antiproliferative activity measured in the NCI-60 differs by cell line. Furthermore, antitumor agents with similar mechanisms of action can produce similar patterns of differential antiproliferative data. We used the matrix COMPARE algorithm[29] to measure the correlations between compounds **4b**, **4c**, **4d**, and **4e** with respect to differential antiproliferative activity. The matrix produced by the analysis showed that **4c** and **4d** have highly correlated activities (r = 0.968) (Table 4). On the contrary, **4e** (the most potent compound tested in the NCI-60) had low correlations (r < 0.5) with the other three compounds. These matrix COMPARE results suggest that **4c** and **4d** have the same mechanism of action, but the mechanism of **4e** is distinct. Future studies will further investigate the importance of the *meta*-phenoxy substituent found in **4e** for its mechanism action. In the studies reported here, we focused on **4e** and related analogs, which also have the *meta*-phenoxy substituent, because of their superior potency.

The COMPARE algorithm can also compare the differential antiproliferative activity of a new compound to those of compounds with known mechanisms of action in the NCI Standard Agent Database.[31] Standard COMPARE analysis has been used previously to identify the cellular targets of antitumor agents.[32] Thus, the pattern of differential antiproliferative activity of **4e** was used to probe the NCI Standard Agent Database for correlations. We used all three measures of activity provided by the NCI-60 screen (GI_{50}, 50% growth inhibition; TGI, total growth inhibition; and LC_{50}, 50% lethal concentration). A standard COMPARE analysis of **4e** (Table 5) showed correlations to paclitaxel, maytansine, vincristine, vinblastine, and rhizoxin, all of which affect microtubule polymerization. Given this *in silico* result, we hypothesized that **4e** targets microtubules and directly tested this hypothesis in vitro. In contrast, the first-ranked COMPARE hits for **4b**–**d** did not include antimicrotubule agents (see Supplemental Information).

Inhibition of Tubulin Polymerization In Vitro

The polymerization of microtubules from purified tubulin can be monitored in vitro by measuring an increase in light scattering. This in vitro experiment removes complicating factors, such as microtubule-associated proteins (MAPs), which might be part of a putative target that leads to disruption of microtubules as observed with microscopy. In order to test our hypothesis that the target of the *N*-((1-benzyl-1*H*-1,2,3-triazol-4-yl)methyl)arylamide scaffold is tubulin, and not a MAP, we monitored the polymerization of tubulin after treatment with **4e**, **13a**, and **13e** (Figure 2). In this experiment, paclitaxel, a microtubule stabilizer, enhanced the rate of tubulin polymerization, while nocodazole, a microtubule

destabilizer, prevented the polymerization of tubulin. Similar to nocodazole, **4e**, **13a**, and **13e** completely inhibited tubulin polymerization at 10 μM. Thus, the triazole-based compounds prevent the formation of microtubules in vitro. We followed this in vitro assay with cell culture experiments to see if microtubules are the primary cellular target.

Cell Cycle Analysis Demonstrated G_2/M-Phase Arrest

Antimicrotubule agents induce M-phase arrest. Flow cytometry can quantitatively determine the population of cells in each phase of the cell cycle by measuring the DNA content of individual cells. Cells in G_2-phase or M-phase have twice as much DNA as cells in G_1-phase. Thus, we conducted flow cytometric cell cycle analysis of HeLa cells treated with **4e**, **13a**, **13d**, **13e**, and **14**. Consistent with the hypothesized mechanism of action, compounds **4e**, **13a**, **13d**, and **13e** significantly increased the population of cells in G_2/M-phase (Figure 3). Upon treatment with these four compounds, the population of G_2/M-phase cells increased from 13% in the control to over 90%. Compound **14**, however, did not induce significant G_2/M-phase arrest, which suggested that the arylamide moiety is important for the antimitotic activity of the *N*-((1-benzyl-1*H*-1,2,3-triazol-4-yl)methyl)arylamide scaffold.

Confocal Microscopy Showed M-phase Arrest and Disruption of Microtubules

Visual evidence for M-phase arrest can be obtained with confocal microscopy due to DNA condensation resulting in enhanced staining by propidium iodide. This outcome is in contrast to the diffuse staining of DNA in interphase cells. Visual evidence for the disruption of microtubules can be obtained concurrently using a fluorescein isothiocyanate-conjugated anti-tubulin antibody. We therefore used confocal microscopy to examine HeLa cancer cells treated with compounds **4e** and **13e**. Both DNA condensation and disruption of microtubules were observed at 5 μM of **4e** or **13e** (Figure 4). Together, these images show that **4e** and **13e** induce M-phase arrest and interfere with microtubule formation in whole cells.

Conclusion

In summary, we identified *N*-((1-benzyl-1*H*-1,2,3-triazol-4-yl)methyl)arylamide as a novel and proprietary[33] small molecule scaffold for potential antitumor agents. Elucidating structure–activity relationships by subtraction from initial hit compound **4e** (MCF-7 IC_{50} = 560 nM) led to the discovery of **13e** (MCF-7 IC_{50} = 46 nM), a foundational compound for further study. Compound **13e** (and related compounds) induced M-phase arrest in HeLa cells at 5 μM and inhibited tubulin polymerization in vitro at 10 μM, providing strong support for antimicrotubule activity as the primary mechanism of action. The NCI-60 screen demonstrated broad-spectrum antitumor activity and prompted further biological evaluation. Compound **13c** was recently evaluated by the National Cancer Institute Developmental Therapeutics Program (NCI DTP) for acute toxicity in vivo, and 100, 200 and 400 mg/kg intraperitoneal (IP) doses were well tolerated in non-tumor bearing mice. Ongoing studies in collaboration with the NCI DTP will evaluate in vivo efficacy in hollow fiber assays.[34] Extensive SAR studies and the development of a combinatorial library are accessible because compounds based on the *N*-((1-benzyl-1*H*-1,2,3-triazol-4-yl)methyl)arylamide scaffold are readily synthesized with the CuAAC reaction. Our findings will facilitate the design and optimization of potent, cell-permeable antimicrotubule agents.

Experimental Section

2-(4-methoxyphenyl)-N-((1-(3-phenoxybenzyl)-1H-1,2,3-triazol-4-yl)methyl)oxazole-4-carboxamide ($C_{27}H_{23}N_5O_4$, 13c)

2-(4-Methoxyphenyl)oxazole-4-carboxylic acid (**11c**, 0.951 g, 4.3 mmol) was suspended in anhydrous CH_2Cl_2 (12 mL) under argon. Oxalyl chloride (0.45 mL, 5.2 mmol) and *N*,*N*-

dimethylformamide (20 μL) were added carefully to the mixture because of gas evolution. The reaction slowly turned to a light yellow homogeneous solution over 3 h. The solution was concentrated *in vacuo* to give 2-(4-methoxyphenyl)oxazole-4-carbonyl chloride (1.0 grams, 97%) as an yellow solid, which was used immediately in the next reaction without characterization.

2-(4-Methoxyphenyl)oxazole-4-carbonyl chloride (1.0 g, 4.0 mmol) was dissolved in anhydrous CH_2Cl_2 (15 mL) under argon and cooled to 0 °C (ice bath). Propargyl amine hydrochloride (0.443 g, 4.8 mmol) and *N*,*N*-diisopropylethylamine (2.1 mL, 12.0 mmol) were added with stirring. The reaction was allowed to warm to room temperature. After stirring for 20 h, TLC analysis indicated completion of the reaction. The mixture was poured into a solution of 10% aqueous $NaHCO_3$ and extracted with CH_2Cl_2 (2x). The organic layer was separated, washed with 10% aqueous $NaHCO_3$ and brine, dried with Na_2SO_4, filtered, and concentrated *in vacuo*. The resultant crude material was purified by column chromatography (SiO_2, EtOAc/CH_2Cl_2 stepwise elution, 1:1 to 10:1) to give 2-(4-Methoxyphenyl)-*N*-(prop-2-ynyl)oxazole-4-carboxamide (**12c**) as an off white solid (0.788 g, 77%). mp 151–152 °C; ^{1}H NMR (300 MHz, $CDCl_3$) δ 8.06 (s, 1H), 7.82 (d, *J* = 8.5 Hz, 2H), 7.13 (bs, NH, 1H), 6.84 (d, *J* = 8.5 Hz, 2H), 4.15−4.07 (m, 2H), 3.72 (s, 3H), 2.15 (s, 1H); ^{13}C NMR (126 MHz, $CDCl_3$) δ 161.82, 161.57, 160.40, 140.49, 136.44, 128.83, 128.29, 119.13, 114.26, 113.69, 79.17, 71.69, 55.37, 28.66; HRMS–FAB (m/z) $[M+H]^+$ calcd for $C_{14}H_{12}N_2O_3$, 257.0921; found, 257.0930.

2-(4-Methoxyphenyl)-*N*-(prop-2-ynyl)oxazole-4-carboxamide (**12c**, 300 mg, 1.17 mmol) and 1-(azidomethyl)-3-phenoxybenzene (290 mg, 1.29 mmol) were suspended in a 2:1 mixture of water and *tert*-butyl alcohol (4.7 mL total volume). Sodium ascorbate (0.12 mmol, 0.12 mL, 1 M) and copper(II) sulfate (0.012 mmol, 0.12 mL, 0.1 M) were added sequentially. After stirring for 4 days at room temperature, TLC analysis indicated complete consumption of the reactants. The reaction mixture was diluted with water (5 mL) and cooled on ice. The white precipitate was isolated by vacuum filtration and washed with cold water (3 × 5 mL) and cold diethyl ether (3 × 3 mL) to afford 506 mg (90%) of pure product (**13c**) as a white powder. TLC R_f = 0.42 (EtOAc); HPLC t_r = 6.82 min (9:1 hexanes/2-propanol); m.p. 119.1 – 119.4 °C; ^{1}H NMR (300 MHz, $CDCl_3$) δ 8.18 (s, 1 H), 7.99 − 7.93 (m, 2 H), 7.60 (bs, NH, 1 H), 7.55 (s, 1 H), 7.39 − 7.28 (m, 3 H), 7.16 − 7.09 (m, 1 H), 7.03 − 6.90 (m, 7 H), 5.47 (s, 2 H), 4.72 (d, J=6.1 Hz, 2 H), 3.88 (s, 3 H); ^{13}C NMR (151 MHz, $CDCl_3$) δ 161.83, 161.56, 160.84, 158.04, 156.36, 145.05, 140.26, 136.70, 136.29, 130.46, 129.85, 128.31, 123.79, 122.46, 122.27, 119.26, 119.18, 118.56, 118.04, 114.28, 55.40, 53.84, 34.46. HRMS–FAB (m/z) $[M+H]^+$ calcd for $C_{27}H_{23}N_5O_4$, 482.1823; found, 482.1803.

Supplementary Material

Refer to Web version on PubMed Central for supplementary material.

Abbreviations

CuAAC	copper-catalyzed azide–alkyne cycloaddition
MIC	minimum inhibition concentration to kill 90% of the bacterium
GI_{50}	50% growth inhibition
TGI	total growth inhibition
LC_{50}	50% lethal concentration, IC_{50}, half maximal inhibitory concentration

TB	*Mycobacterium tuberculosis*
GAST	medium of glycerol-alanine-salts-Tween 80 without added iron
DBU	1,8-Diazabicyclo[5.4.0]undec-7-ene
S.E.M.	standard error of the mean

Acknowledgments

Initial support by the NIH (R01 AI 05419) of the antituberculosis research program that generated the lead compounds is gratefully acknowledged. We would like to thank the University of Notre Dame especially the Mass Spectrometry & Proteomics Facility (Bill Boggess, Nonka Sevova, Michelle Joyce) which is supported by the by Grant CHE-0741793 from the National Science Foundation and Dr. Jaroslav Zajicek for assistance in obtaining mass spectral and NMR data, respectively. We thank Dr. Kamlesh Gupta and Prof. Holly Goodson for advice regarding the tubulin experiments and Dr. Timothy Mitchison for the gift of purified tubulin. We also thank Dr. Jed Fisher for helpful discussions. We acknowledge financial support from the University of Notre Dame (J.A.S. was supported by a Notre Dame College of Science Summer Undergraduate Research Fellowship). We would also like to acknowledge the assistance of the Cell Flow Cytometry facility of the Biotechnology Center at the University of Illinois at Urbana-Champaign.

References

1. Jordan MA, Wilson L. Microtubules as a Target for Anticancer Drugs. Nat. Rev. Cancer 2004;4:253–265. [PubMed: 15057285]
2. (a) Mitchison TJ. Microtubule Dynamics and Kinetochore Function in Mitosis. Annu. Rev. Cell Biol 1988;4:527–549. [PubMed: 3058165] (b) Rusan NM, Fagerstrom CJ, Yvon AC, Wadsworth P. Cell Cycle-Dependent Changes in Microtubule Dynamics in Living Cells Expressing Green Fluorescent Protein-α Tubulin. Mol. Biol. Cell 2001;12:971–980. [PubMed: 11294900]
3. Jordan MA. Mechanism of Action of Antitumor Drugs that Interact with Microtubules and Tubulin. Curr. Med. Chem. – Anti-Cancer Agents 2002;2:1–17.
4. (a) Islam MN, Iskander MN. Microtubulin Binding Sites as Target for Developing Anticancer Agents. Mini-Reviews in Medicinal Chemistry 2004;4:1077–1104. [PubMed: 15579115] (b) Hadfield JA, Ducki S, Hirst N, McGown AT. Tubulin and Microtubules as Targets for Anticancer Drugs. Progress in Cell Cycle Research 2003;5:309–325. [PubMed: 14593726] (c) Hamel E. Antimitotic Natural Products and Their Interactions with Tubulin. Med. Res. Rev 1996;16:207–231. [PubMed: 8656780]
5. Hanahan D, Weinberg RA. The Hallmarks of Cancer. Cell 2000;100:57–70. [PubMed: 10647931]
6. Kuppens IELM. Current State of the Art of New Tubulin Inhibitors in the Clinic. Curr. Clin. Pharmacol 2006;1:57–70. [PubMed: 18666378]
7. (a) Jordan A, Hadfield JA, Lawrence NJ, McGown AT. Tubulin as a Target for Anticancer Drugs: Agents Which Interact with the Mitotic Spindle. Med. Res. Rev 1998;18:259–296. [PubMed: 9664292] (b) Kiselyov A, Balakin KV, Tkachenko SE, Savchuk N, Ivachtchenko AV. Recent Progress in Discovery and Development of Antimitotic Agents. Anti-Cancer Agents in Med. Chem 2007;7:189–208.
8. Backer G, Beckers T, Emig P, Klenner T, Kutscher B, Nickel B. New small-molecule tubulin inhibitors. Pure Appl. Chem 2001;73:1459–1464.
9. Wood KW, Cornwell WD, Jackson JR. Past and future of the mitotic spindle as an oncology target. Curr. Opin. Pharmacol 2001;1:370–377. [PubMed: 11710735]
10. (a) Snow GA. Mycobactins: Iron-Chelating Growth Factors from Mycobacteria. Bacteriol. Rev 1970;34:99–125. [PubMed: 4918634] (b) White AJ, Snow GA. Isolation of Mycobactins form Various Mycobacteria: The Properties of Mycobactins S and H. Biochem. J 1969;111:785–792. [PubMed: 5783478]
11. (a) Maurer PJ, Miller MJ. Total Synthesis of a Mycobactin: Mycobactin S2. J. Am. Chem. Soc 1983;105:240–245. (b) Hu J, Miller MJ. Total Synthesis of a Mycobactin S, a Siderophore and

Growth Promoter of *Mycobacterium Smegmatis*, and Determination of its Growth Inhibitory Activity against *Mycobacterium tuberculosis*. J. Am. Chem. Soc 1997;119:3462–3468.

12. Vergne AF, Walz AJ, Miller MJ. Iron chelators from mycobacteria (1954–1999) and potential therapeutic applications. Nat. Prod. Rep 2000;17:99–116. [PubMed: 10714901]
13. (a) Moraski GC, Chang M, Villegas-Estrada A, Franzblau S, Möllmann U, Miller MJ. Structure-Activity Relationship of New Antituberculosis Agents Derived from Oxazoline and Oxazole Benzyl Esters. Eur. J. Med. Chem. 2010 in press. (b) Moraski GC, Franzblau SG, Miller M. Utilization of the Suzuki Coupling to Enhance the Antituberculosis Activity of Aryl Oxazoles. Heterocyles 2010;80:977–988.
14. Fennell KA, Miller MJ. Synthesis of Amamistatin Fragments and Determination of Their HDAC and Antitumor Activity. Org. Lett 2007;9:1683–1685. [PubMed: 17397173]
15. Siddiquee KAZ, Gunning PT, Glenn M, Katt WP, Zhang S, Schroeck C, Sebti SM, Jove R, Hamilton AD, Turkson J. An Oxazole-Based Small-Molecule Stat3 Inhibitor Modulates Stat3 Stability and Processing and Induces Antitumor Cell Effects. ACS Chem. Biol 2007;2:787–798. [PubMed: 18154266]
16. Kuang R, Shue HJ, Blythin DJ, Shih NY, Gu D, Chen X, Schwerdt J, Lin L, Ting PC, Zhu X, et al. Discovery of a highly potent series of oxazole-based phosphodiesterase 4 inhibitors. Bioorg. Med. Chem. Lett 2007;17:5150–5154. [PubMed: 17683932]
17. (a) Rice RL, Rusnak JM, Yokokawa F, Yokokawa S, Messner DJ, Boynton AL, Wipf P, Lazo JS. A Targeted Library of Small-Molecule, Tyrosine, and Dual-Specificity Phosphatase Inhibitors Derived from a Rational Core Design and Random Side Chain Variation. Biochemistry 1997;36:15965–15974. [PubMed: 9398331] (b) Ducruet AP, Rice RL, Tamura K, Yokokawa F, Yokokawa S, Wipf P, Lazo JS. Identification of New Cdc25 Dual Specificity Phosphatase Inhibitors in a Targeted Small Molecule Array. Bioorg. Med. Chem 2000;8:1451–1466. [PubMed: 10896122]
18. Takeuchi K, Kohn TJ, True TA, Mais DE, Wikel JH, Utterback BG, Wyss VL, Jakubowski JA. Development of Dual-Acting Agents for Thromboxane Receptor Antagonism and Thromboxane Synthase Inhibition. 3. Synthesis and Biological Activities of Oxazolecarboxamide-Substituted ω-Phenyl-ω-(3-pyridyl)alkenoic Acid Derivatives and Related Compounds. J. Med. Chem 1998;41:5362–5374. [PubMed: 9876106]
19. Morwick T, Berry A, Brickwood J, Cardozo M, Catron K, DeTuri M, Emeigh J, Homon C, Hrapchak M, Jacober S. Evolution of the Thienopyridine Class of Inhibitors of IκB Kinase-β: Part I: Hit-to-Lead Strategies. J. Med. Chem 2006;49:2898–2908. [PubMed: 16686533]
20. Tai VWF, Sperandio D, Shelton EJ, Litvak J, Pararajasingham K, Cebon B, Lohman J, Eksterowicz J, Kantak S, Sabbatini P, et al. Discovery and structure-activity relationship of 2-phenyl-oxazole-4-carboxamide derivatives as potent apotosis inducers. Bioorg. Med. Chem. Lett 2006;16:4554–4558. [PubMed: 16784854]
21. GAST medium is glycerol-alanine-salts-Tween 80 medium without added iron. See, (a) Voss JJD, Rutter K, Schroeder BG, Su H, Zhu Y, Barry CE. The salicylate-derived mycobactin siderophores of *Mycobacterium tuberculosis* are essential for growth in macrophages. Proc. Natl. Acad. Sci. USA 2000;97:1252–1257. [PubMed: 10655517] (b) Cho SH, Warit S, Wan B, Hwang CH, Pauli GF, Franzblau SG. Low-Oxygen-Recovery Assay for High-Throughput Screening of Compounds against Nonreplicating Mycobacterium tuberculosis. Antimicrob. Agents Chemother 2007;51:1380–1385. [PubMed: 17210775]
22. Phillips AJ, Uto Y, Wipf P, Reno MJ, Williams DR. Synthesis of Functionalized Oxazolines and Oxazoles with DAST and Deoxo-Fluor. Org. Lett 2000;2:1165–1168. [PubMed: 10804580]
23. (a) Kolb HC, Finn MG, Sharpless KB. Click Chemistry: Diverse Chemical Function from a Few Good Reactions. Angew. Chem. Int. Ed 2001;40:2004–2021. (b) Moses JE, Moorhouse AD. The Growing Applications of Click Chemistry. Chem. Soc. Rev 2007;36:1249–1262. [PubMed: 17619685]
24. (a) Rostovtsev VV, Green LG, Fokin VV, Sharpless KBA. Stepwise Huisgen Cycloaddition Process: Copper(I)-Catalyzed Regioselective “Ligation” of Azides and Terminal Alkynes. Angew. Chem. Int. Ed 2002;41:2596–2599. (b) Tornøe CW, Christensen C, Meldal M. Peptidotriazoles on Solid Phase: [1,2,3]-Triazoles by Regiospecific Copper(I)-Catalyzed 1,3-Dipolar Cycloadditions of Terminal Alkynes to Azides. J. Org. Chem 2002;67:3057–3064. [PubMed: 11975567]

25. Kolb HC, Sharpless KB. The Growing Impact of Click Chemistry on Drug Discovery. Drug Discovery Today 2003;8:1128–1137. [PubMed: 14678739]
26. Alvarez SG, Alvarez MT. A Practical Procedure for the Synthesis of Alkyl Azides at Ambient Temperature in Dimethyl Sulfoxide in High Purity and Yield. Synthesis 1997;4:413–414.
27. (a) Boyd MR, Paull KD. Some Practical Considerations and Applications of the National Cancer Institute In Vitro Anticancer Drug Discovery Screen. Drug Develop. Res 1995;34:91–109. (b) Shoemaker RH. The NCI60 Human Tumor Cell Line Anticancer Drug Screen. Nature Rev. Cancer 2006;6:813–823. [PubMed: 16990858]
28. (a) Ross DT, Scherf U, Eisen MB, Perou CM, Rees C, Spellman P, Iyer V, Jeffrey SS, Van de Rijn M, Waltham M, Pergamenschikov A, Lee JCF, Lashkari D, Shalon D, Myers TG, Weinstein JN, Botstein D, Brown PO. Systematic variation of gene expression patterns in human cancer cell lines. Nature Genetics 2000;24:227–235. [PubMed: 10700174] (b) Ellison G, Klinowska T, Westwood RFR, Docter E, French T, Fox JC. Further evidence to support the melanocytic origin of MDA-MB-435. J. Clin. Pathol: Mol. Pathol 2002;55:294–299.
29. (a) Paull KD, Shoemaker RH, Hodes L, Monks A, Scudiero DA, Rubinstein L, Plowman J, Boyd MR. Display and Analysis of Patterns of Differential Activity of Drugs Against Human Tumor Cell Lines: Development of Mean Graph and COMPARE Algorithm. J. Natl. Cancer Inst 1989;81:1088–1092. [PubMed: 2738938] (b) Zaharevitz DW, Holbeck SL, Bowerman C, Svetlik PA. COMPARE: a web accessible tool for investigating mechanisms of cell growth inhibition. J. Mol. Graphics Modell 2002;20:297–303.
30. (a) Paull KD, Shoemaker RH, Hodes L, Monks A, Scudiero DA, Rubinstein L, Plowman J, Boyd MR. Display and Analysis of Patterns of Differential Activity of Drugs Against Human Tumor Cell Lines: Development of Mean Graph and COMPARE Algorithm. J. Natl. Cancer Inst 1989;81:1088–1092. [PubMed: 2738938] (b) Zaharevitz DW, Holbeck SL, Bowerman C, Svetlik PA. COMPARE: a web accessible tool for investigating mechanisms of cell growth inhibition. J. Mol. Graphics Modell 2002;20:297–303.
31. DTP Human Tumor Cell Line Screen, Standard Agent Database. Online: http://dtp.nci.nih.gov/docs/cancer/searches/standard_agent.html
32. (a) Bai R, Paull KD, Herald CL, Malspeis L, Pettit GR, Hamel E, Halichondrin B, Homohalichondrin B. Marine Natural Products Binding in the Vinca Domain of Tubulin. J. Biol. Chem 1991;266:15882–15889. [PubMed: 1874739] (b) Paull KD, Lin CM, Malspeis L, Hamel E. Identification of Novel Antimitotic Agents Acting at the Tubulin Level by Computer-assisted Evaluation of Differential Cytotoxicity Data. Cancer Res 1992;52:3892–3900. [PubMed: 1617665] (c) Kuo SC, Lee HZ, Juang JP, Lin YT, Wu TS, Chang JJ, Lednicer D, Paull KD, Lin CM, Hamel E, Lee KH. Synthesis and Cytotoxicity of 1,6,7,8-Substituted 2-(4'-Substituted phenyl)-4-quinolones and Related Compounds: Identification as Antimitotic Agents Interacting with Tubulin. J. Med. Chem 1993;36:1146–1156. [PubMed: 8387598]
33. Stefely JA, Moraski GA, Miller MJ. Anti-cancer Compounds, Synthesis Thereof, And Methods Of Using Same. WO/2009/111502.
34. Hollingshead MG, Alley MC, Camalier RF, Abbott BJ, Mayo JG, Malspeis L, Grever MR. *In vivo* cultivation of tumor cells in hollow fibers. Life Sci 1995;57:131–141. [PubMed: 7603295]

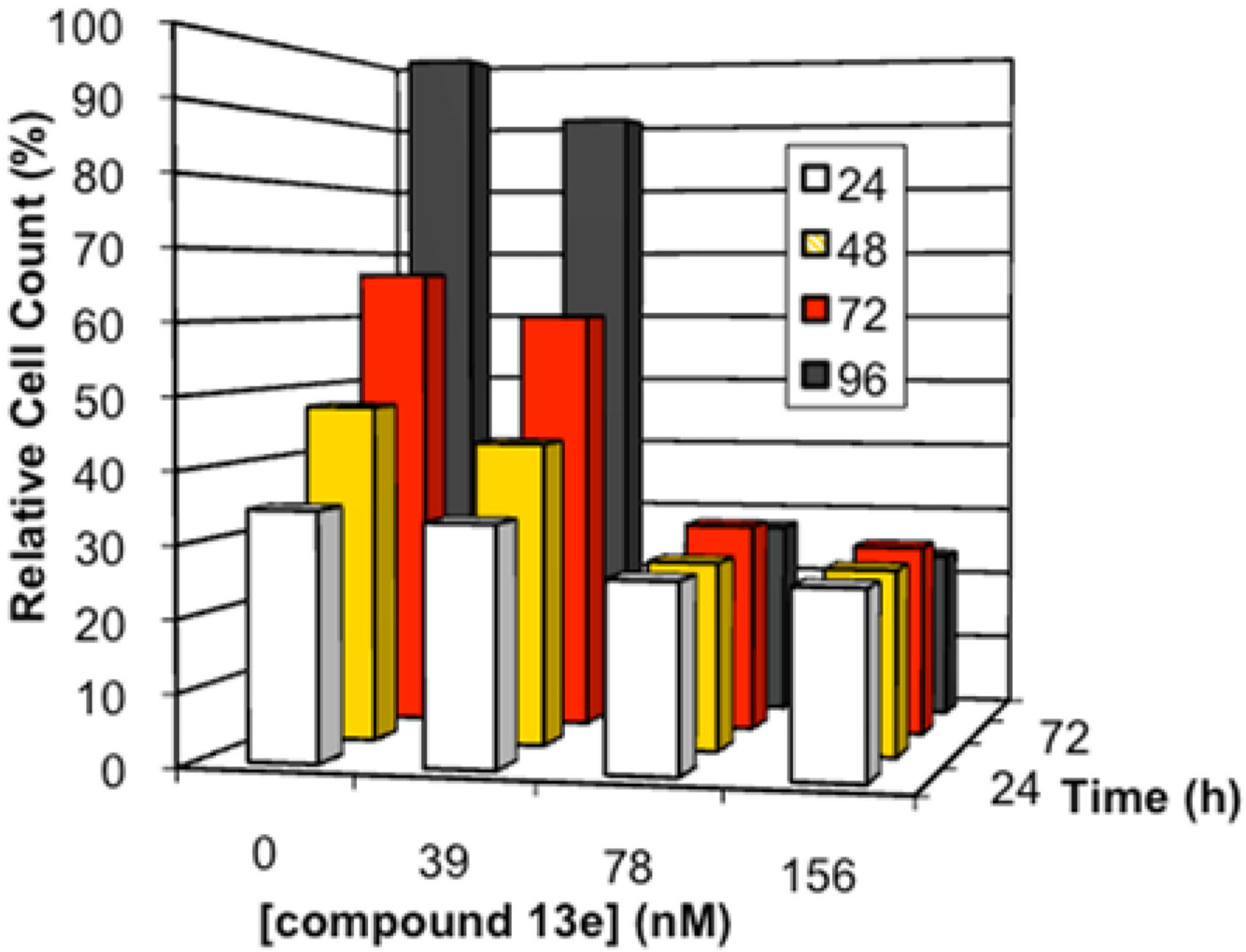

Figure 1.
Time and concentration dependence of the antiproliferative activity of **13e** against MCF-7 tumor cells. Time is in terms of time elapsed after addition of the compound. Cell counts are shown relative to the cell count observed in the vehicle control 96 h after addition of the 0.5% DMSO solution.

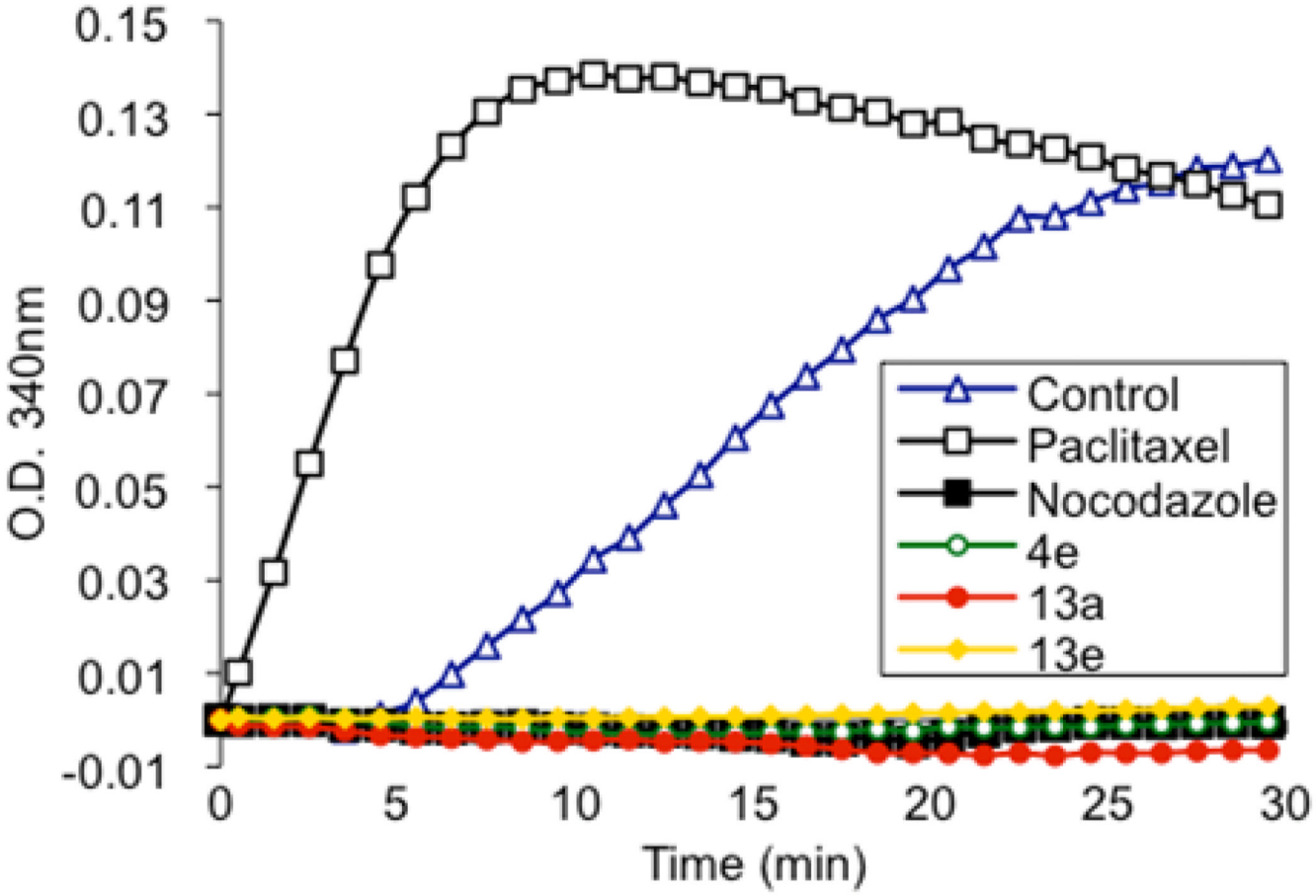

Figure 2.
Inhibition of tubulin assembly by **4e**, **13a**, and **13e** in vitro. All compounds were tested at a concentration of 10 μM. Effects of compounds on tubulin polymerization were assessed by monitoring the increase in light scattering, measured as optical density (O.D.), at 340 nm. Standards of 10 μM nocodazole (a tubulin assembly inhibitor) and 10 μM paclitaxel (a tubulin assembly promoter) were used for direct comparison.

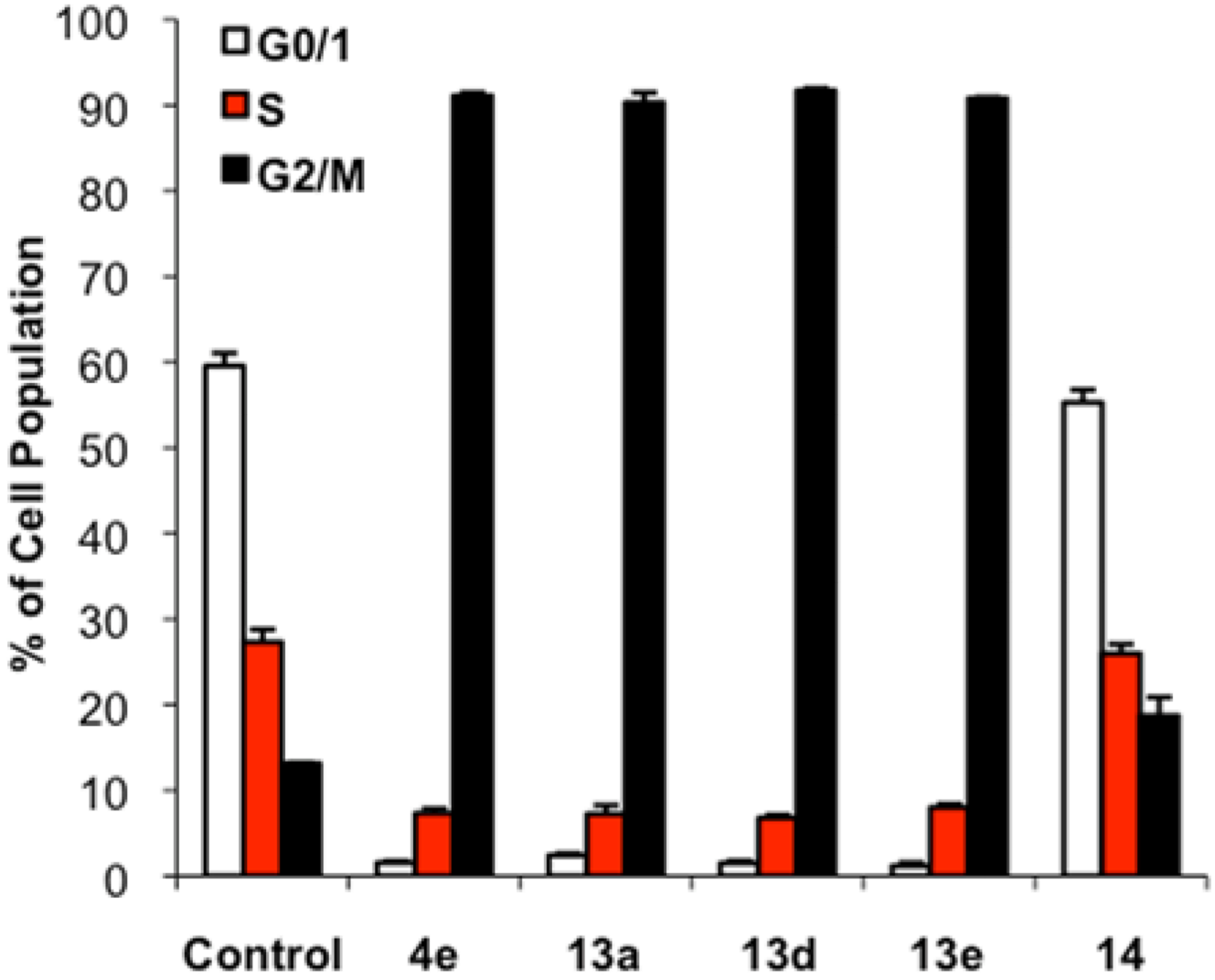

Figure 3.
Effects of **4e**, **13a**, **13d**, **13e**, and **14** on the cell cycle distribution of HeLa cells as measured by propidium iodide staining and flow cytometry. HeLa cells were treated with 5 μM compound for 18 h in triplicate.

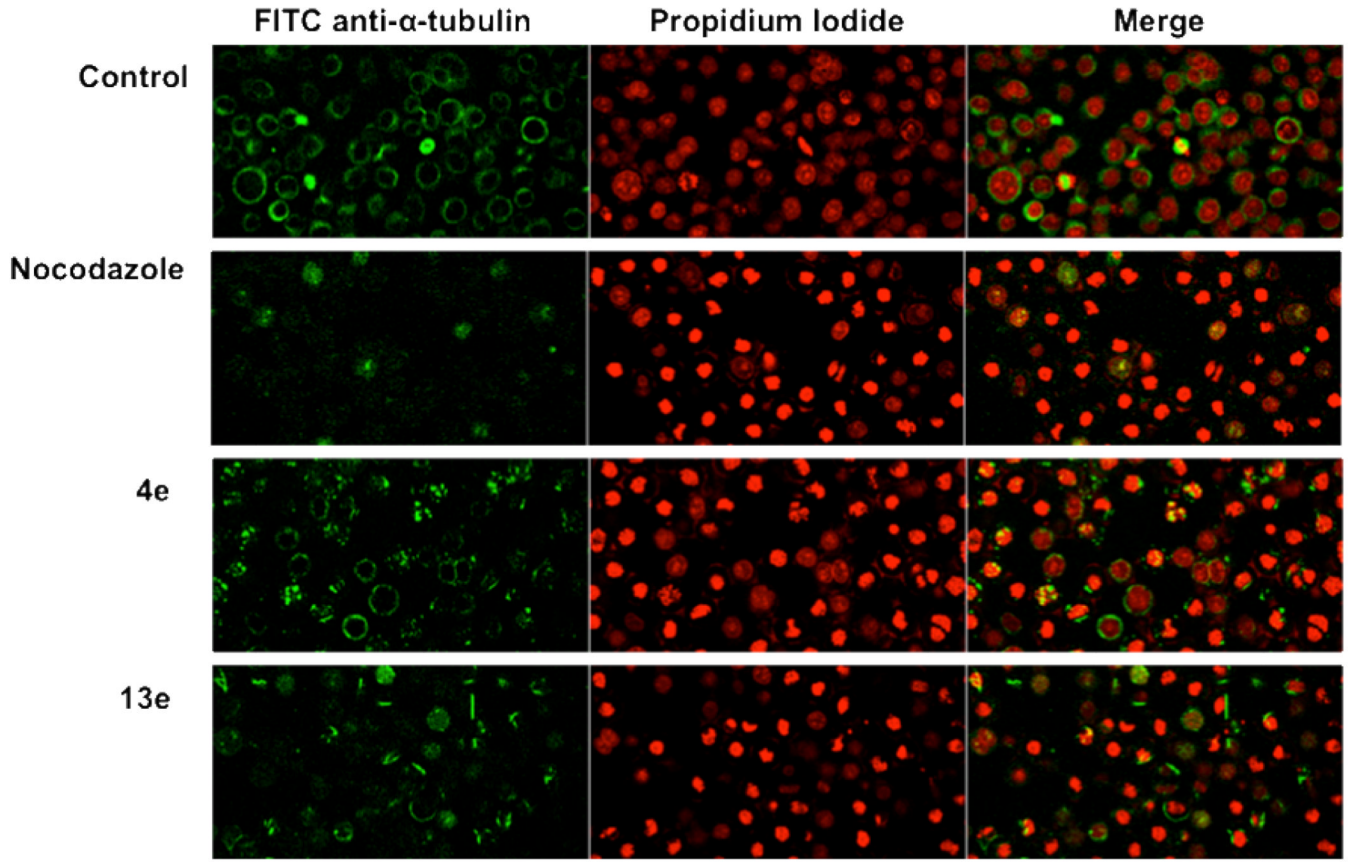

Figure 4.

Confocal microscopy images of HeLa cells after 18 h incubation in the presence of 5 μM compound. Nocodazole is a known tubulin polymerization inhibitor. Nuclear DNA was stained with propidium iodide (red channel) and tubulin was stained with FITC-conjugated anti-α-tubulin antibody (green channel). Compounds **4e** and **13e** disrupted normal microtubule structures, caused fragmentation of mitotic spindles, and induced M-phase arrest.

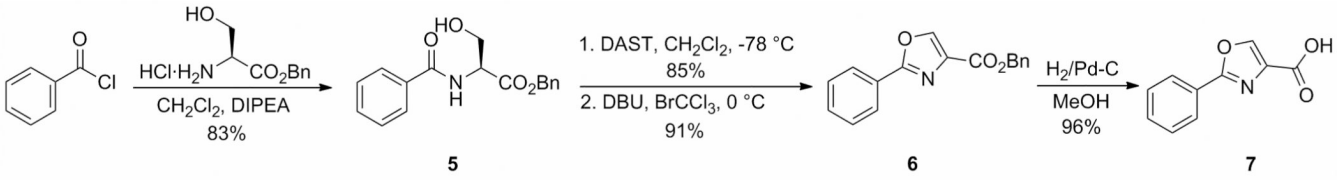

Scheme 1.
Synthesis of 2-phenyloxazole-4-carboxylic acid.

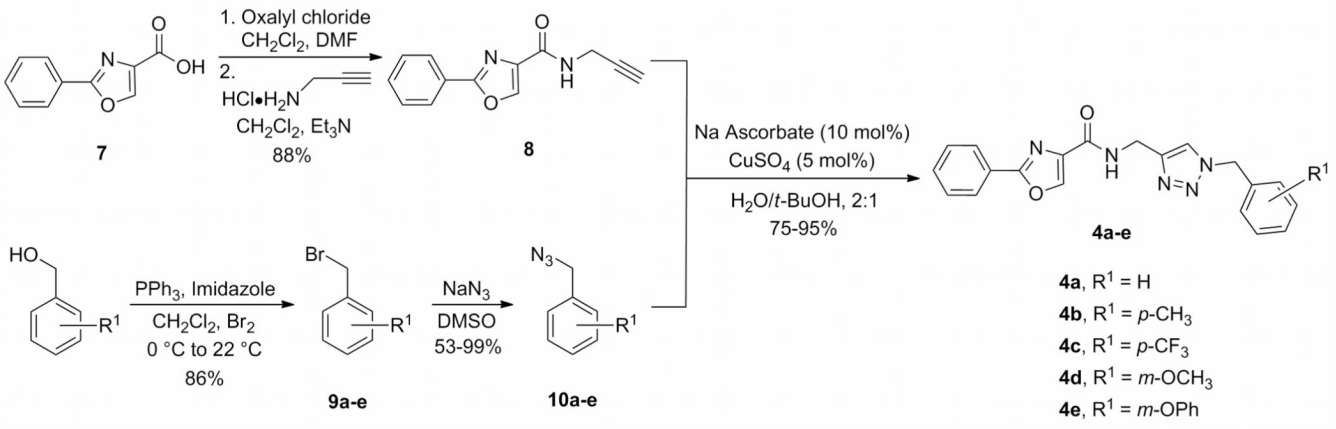

Scheme 2.
Synthesis of *N*-((1-benzyl-1*H*-1,2,3-triazol-4-yl)methyl)-2-phenyl-oxazole-4-carboxamide scaffold.

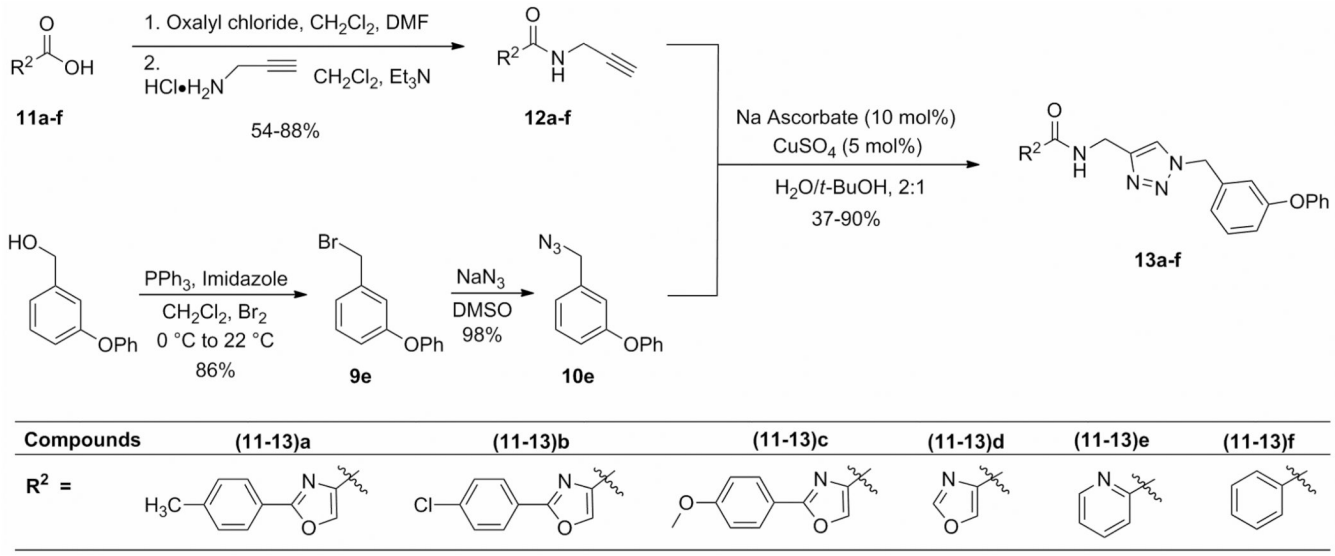

Scheme 3.
Synthesis of *N*-((1-benzyl-1*H*-1,2,3-triazol-4-yl)methyl)arylamide scaffold.

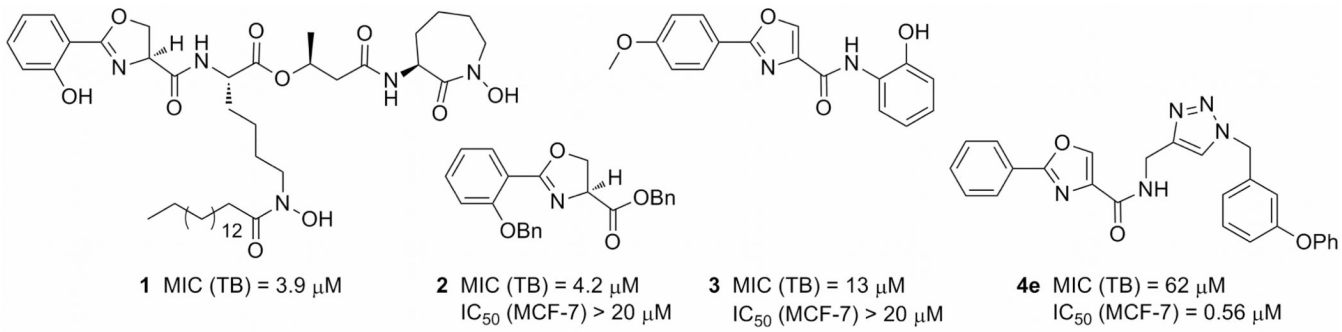

Chart 1.

Structures of anti-tuberculosis compounds **2** and **3** and antimicrotubule compound **4e**, all derived from a fragment of mycobactin S (**1**). MIC values indicate in vitro anti-tuberculosis activity against *M. tuberculosis* H37Rv in GAST medium[21], and IC_{50} values indicate in vitro antiproliferative activity against human breast cancer cell line MCF-7.

Table 1

In vitro antiproliferative activity of compounds **4a**–**e**, colchicine, and 2-methoxyestradiol against human breast cancer cell line MCF-7.

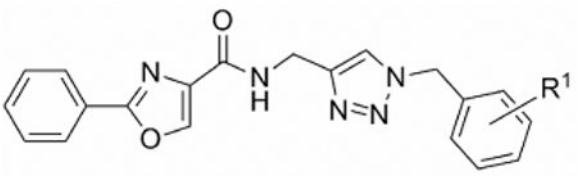

		IC_{50} (μM)
Compound	**R^1**	**MCF-7**
4a	H	15.9
4b	*p*-CH_3	7.59
4c	*p*-CF_3	7.33
4d	*m*-OCH_3	8.35
4e	*m*-OPh	0.56
Colchicine		0.013
2-methoxyestradiol		0.84

Table 2

Antiproliferative activities (IC_{50}) of compounds **4e**, **13a**–**f**, **14**, colchicine, and 2-methoxyestradiol against human breast cancer cell line MCF-7 and human lymphoma cell line U937.

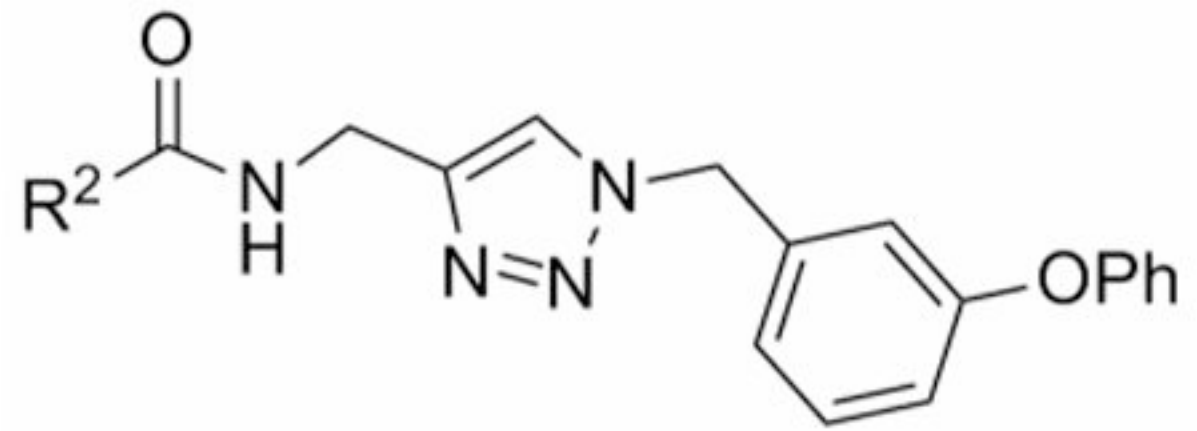

Compound	R^2	
4e	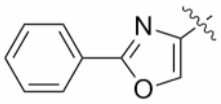	
13a	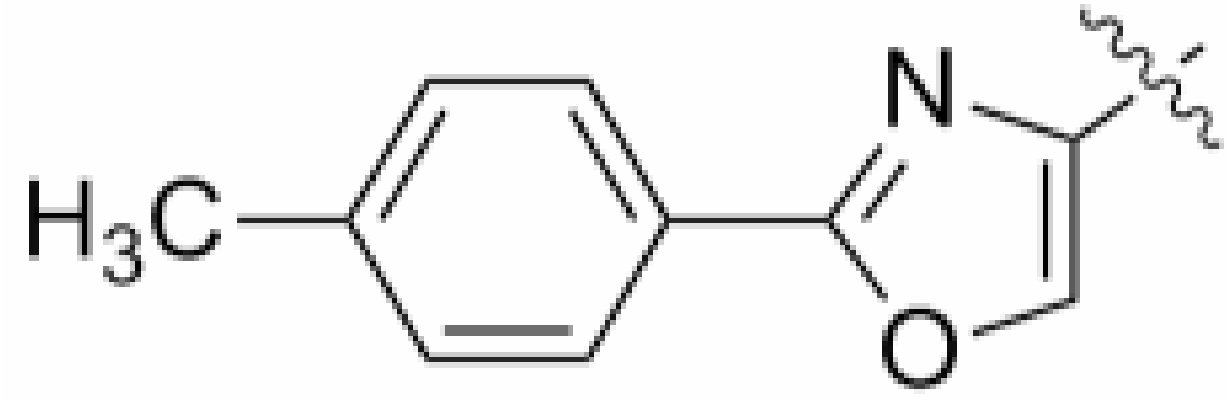	
13b	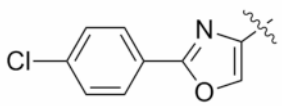	
13c	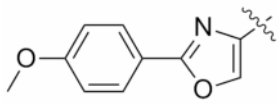	

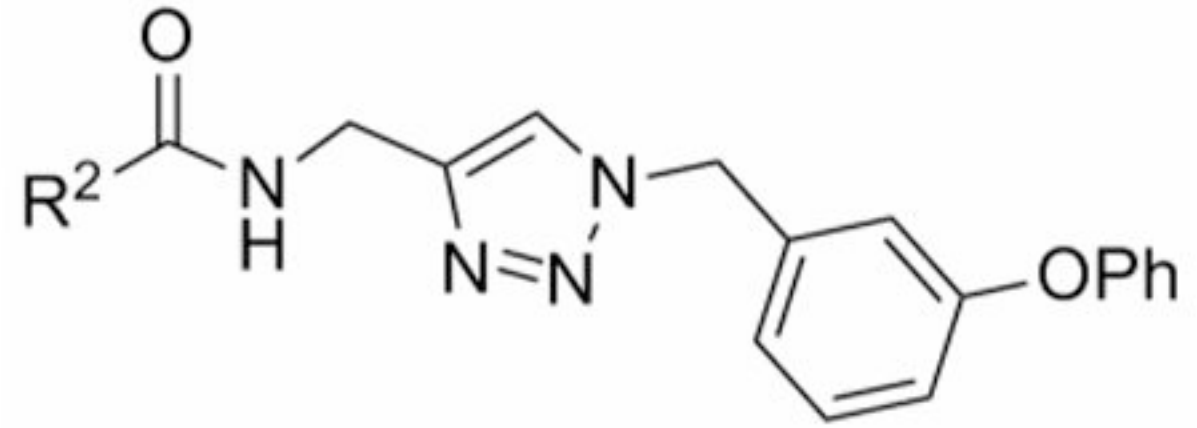

Compound	R2	
13d	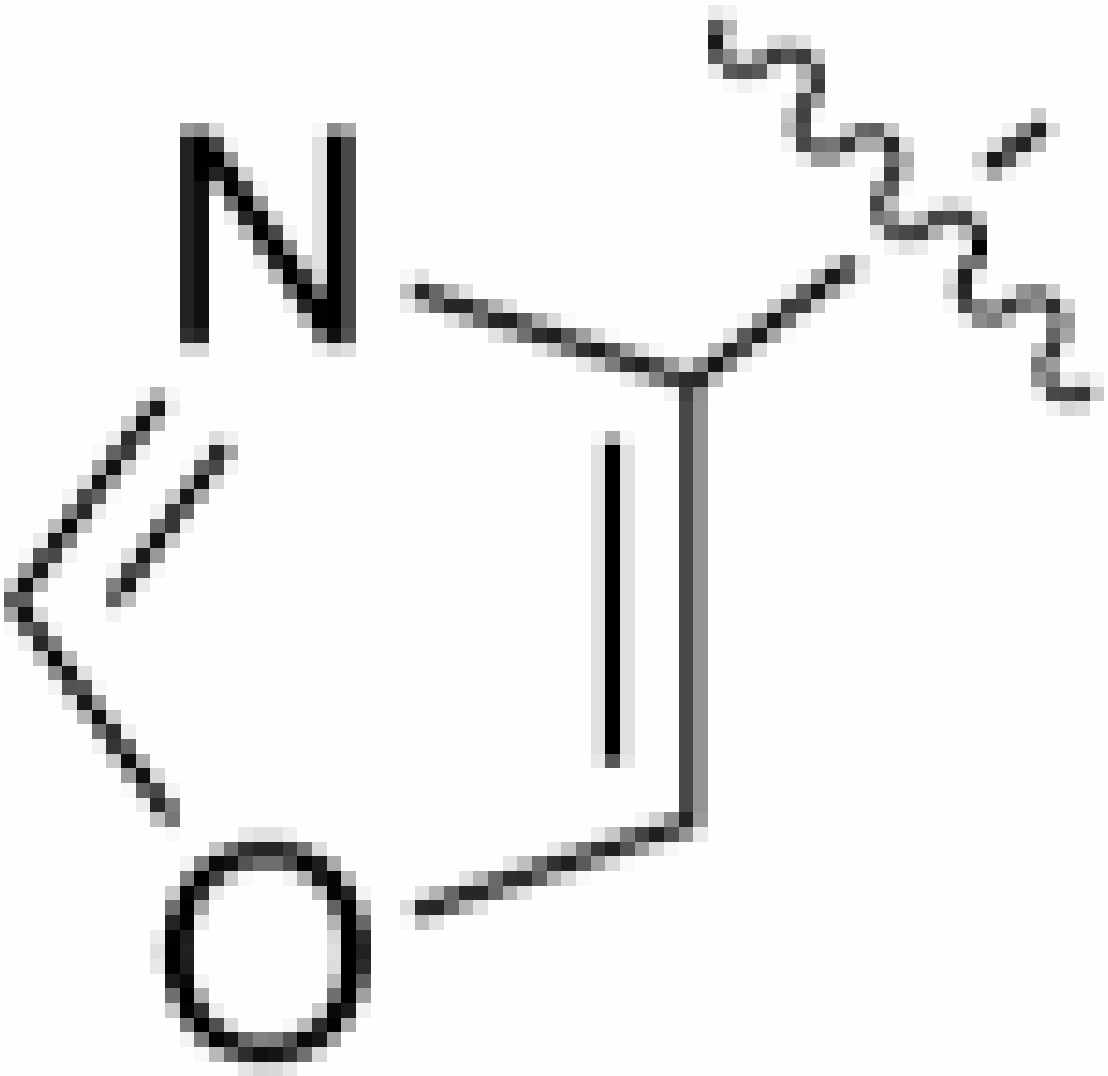	

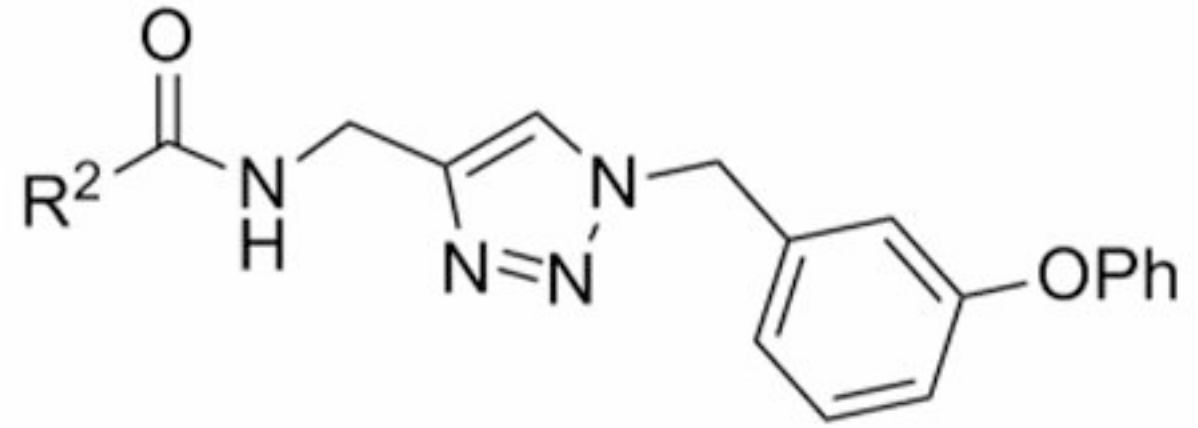

Compound	R^2
13e	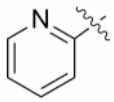

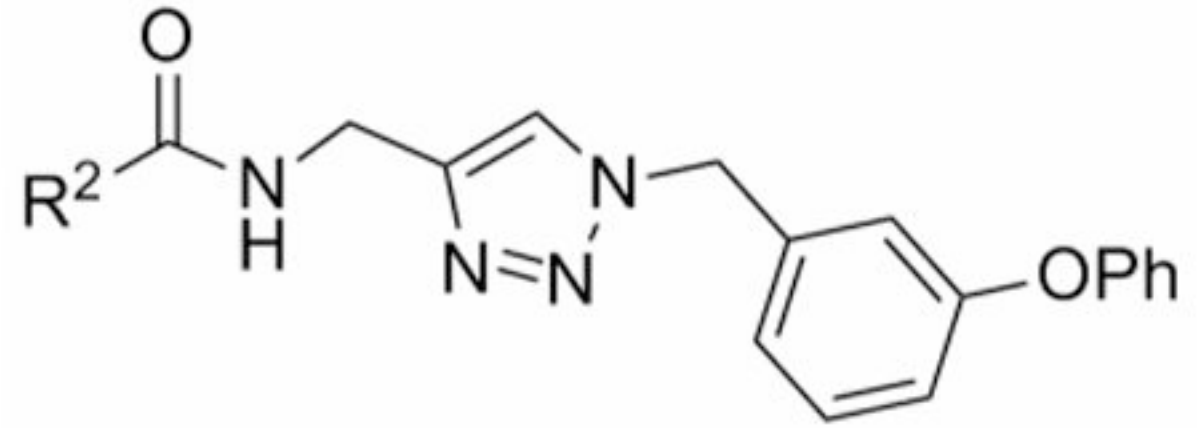

Compound	R2	
13f	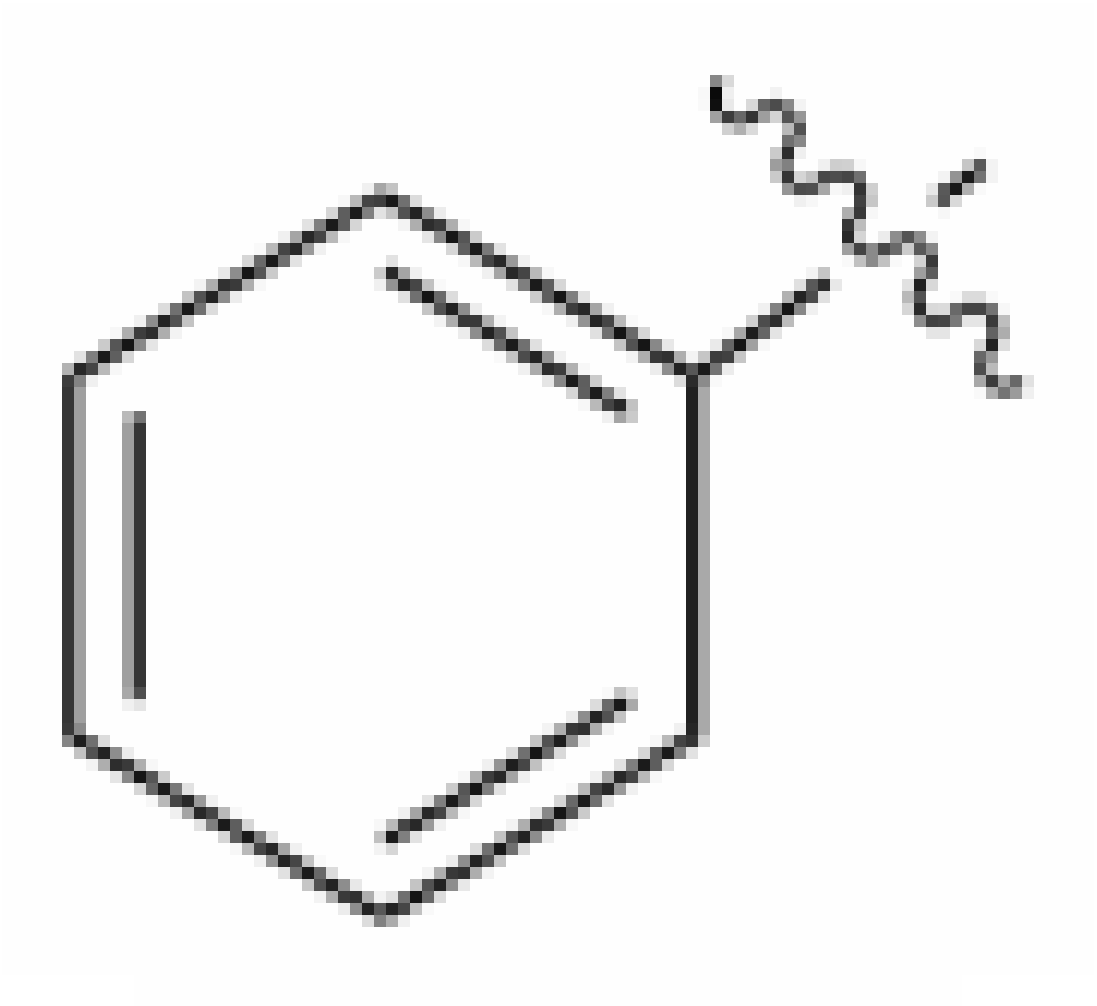	0

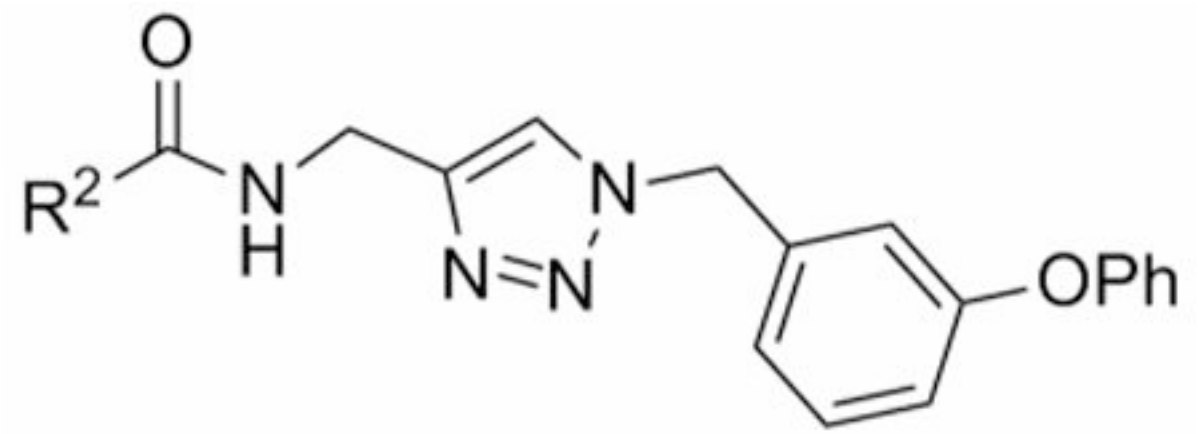

Compound	R2	–
14	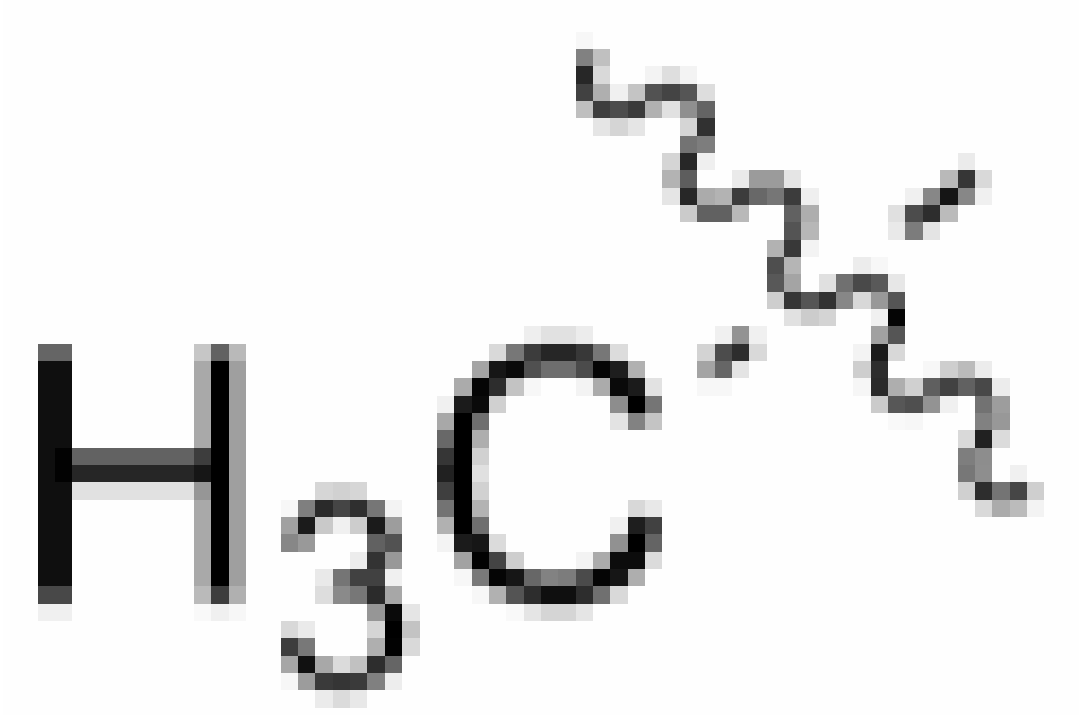	
Colchicine		
2-methoxyestradiol		0

[a] IC_{50} values represent the concentration at which the cell count was inhibited to 50% of that measured in the vehicle control. Error is S.E.M., n≥3.

Table 3

Antiproliferative activity of compounds **4b**, **4c**, **4d**, and **4e** against selected cell lines in the NCI-60 screen.

	GI_{50} (μM)			
compound	**mean**	**HL-60**	**MCF-7**	**MDA-MB-435**
4b	21.9	1.53	8.93	3.71
4c	16.6	2.34	3.83	1.94
4d	17.8	2.37	4.16	2.12
4e	0.87	0.39	0.36	0.18

Table 4

Matrix COMPARE analysis of **4b**, **4c**, **4d**, and **4e**. Matrix values (r values) are Pearson's correlation coefficients.[30]

compound	4b	4c	4d	4e
4b	1.000	0.600	0.583	0.489
4c	0.600	1.000	0.968	0.475
4d	0.583	0.968	1.000	0.491
4e	0.489	0.475	0.491	1.000

Table 5

Standard COMPARE analysis of **4e**. The Target Set was the Standard Agent Database and the Target Set Endpoints were set equal to the Seed Endpoints (GI_{50}, TGI, and LC_{50}). Correlation values (r) are Pearson's correlation coefficients. Some hits appear multiple times because they were tested by the NCI for the Standard Agent Database at multiple concentration ranges.

rank	compound	r
Based on GI_{50} Mean Graph		
1	paclitaxel	0.541
2	maytansine	0.534
3	vincristine sulfate	0.500
4	trimetrexate	0.480
5	soluble Baker's Antifol	0.460
Based on TGI Mean Graph		
1	paclitaxel (hiConc = 10^{-5} M)	0.654
2	paclitaxel (hiConc = 10^{-6} M)	0.646
3	paclitaxel (hiConc = $10^{-4.6}$ M)	0.642
4	maytansine	0.621
5	vinblastine sulfate	0.606
Based on LG_{50} Mean Graph		
1	rhizoxin (hiConc = 10^{-9} M)	0.681
2	rhizoxin (hiConc = 10^{-4} M)	0.650
3	vinblastine sulfate (hiConc = $10^{-7.6}$ M)	0.558
4	α-2'-deoxythioguanosine	0.545
5	vinblastine sulfate (hiConc = 10^{-4} M)	0.540